The molecular switching mechanism at the conserved D(E)RY motif in class-A GPCRs

Sandoval, A.; Eichler, S.; Madathil, S.; Reeves, P. J.; Fahmy, K.; Boeckmann, R. A.;

Originally published:

July 2016

Biophysical Journal 111(2016)1, 79-89

DOI: https://doi.org/10.1016/j.bpj.2016.06.004

The molecular switching mechanism at the conserved E(D)RY motif in class-A GPCRs

Angelica Sandoval[1], Stefanie Eichler[2], Sineej Madathil[2], Philip J. Reeves[3], Karim Fahmy[2,*], and Rainer A. Böckmann[1,*]

[1]Computational Biology, Department of Biology, Friedrich-Alexander Universität Erlangen-Nürnberg, Erlangen, Germany

[2]Helmholtz-Zentrum Dresden - Rossendorf, Institute of Resource Ecology, Dresden, and Technische Universität Dresden, Germany

[3]School of Biological Sciences, University of Essex, UK

Abstract

The disruption of ionic and H-bond interactions between the cytosolic ends of transmembrane helices TM3 and TM6 of class-A (rhodopsin-like) G protein-coupled receptors (GPCRs) is a hallmark for their activation by chemical or physical stimuli. In the photoreceptor rhodopsin, this is accompanied by proton uptake at Glu^{134} in the class-conserved E(D)RY motif. Studies on TM3 model peptides proposed a crucial role of the lipid bilayer in linking protonation to stabilization of an active state-like conformation. However, the molecular details of this linkage could not be resolved and have been addressed here by molecular dynamics (MD) simulations on TM3 model peptides in a DOPC bilayer.

We show that protonation of the conserved glutamic acid alters its side chain rotamer preferences and stabilizes the C-terminal helical structure. Both factors contribute to the rise of the side chain pK_a (> 6) and to reduced polarity around the TM3 C-terminus as confirmed by fluorescence spectroscopy. Helix stabilization requires the protonated carboxyl group; unexpectedly, this stabilization could not be evoked with an amide in MD simulations. Additionally, time-resolved FTIR spectroscopy of TM3 model peptides revealed a different kinetics for lipid ester carbonyl hydration, suggesting that the carboxyl is linked to more extended H-bond clusters than an amide. Remarkably, this was seen as well in DOPC-reconstituted Glu^{134}- and Gln^{134}-containing opsin mutants and demonstrates that

the E(D)RY motif is a hydrated microdomain. The function of the E(D)RY motif as a proton switch is suggested to be based on the reorganization of the H-bond network at the membrane interface.

*correspondence: k.fahmy@hzdr.de and rainer.boeckmann@fau.de

Introduction

G protein-coupled receptors (GPCRs) are a superfamily of membrane proteins that undergo conformational changes in response to extracellular chemical or physical stimuli. The ensuing conformational changes of their seven transmembrane TM helical structure lead to an activated receptor state which catalyzes GDP / GTP exchange in cytosolic G proteins (guanosine nucleotide-binding proteins). More than 600 GPCRs in humans belong to the class-A (1) which is characterized by structural homology with the visual photoreceptor rhodopsin. In contrast to ligand-activated GPCRs, rhodopsin is activated by 11-cis to all-trans photoisomerization of the retinal, which is covalently bound via a protonated Schiff base to the side chain nitrogen of Lys^{296} of the apoprotein opsin (see Fig. 1). Functional studies of bovine rhodopsin have contributed to the identification of critical molecular activation steps that are thought to be shared by class-A GPCRs as has been reviewed in detail (2, 3). It has been shown for the β_2-adrenergic receptor that the breakage of ionic and H-bond interactions which link the cytosolic ends of TM3 and TM6 in the inactive receptor state is crucial for GPCR activation (4–6). Studies on bovine rhodopsin revealed that the corresponding distance increase between TM3 and TM6 (7) is followed by a proton uptake reaction in the side chain of Glu^{134} within the class-conserved E(D)RY motif at the C-terminal end of TM3 (8). This cytosolic 'proton switch' (9, 10) involves the proton exchange with the environment and is thus pH-dependent. It is evoked by preceding light-induced structural changes (11) and internal proton transfer reactions (12) among which the pH-insensitive internal 'proton switch I', i.e., the transfer of the Schiff base proton to its counterion Glu^{113} (13), is the key step that leads to the active metarhodopsin II (MIIa) conformation (14). The following movement of TM6 and TM5 (helices H6 and H5, MIIb state, see Fig. 1 A.1 and B) precedes the protonation at Glu^{134} in the conserved D(E)RY motif at the C-terminal end of TM3 (H3), leading to the $MIIbH^+$ intermediate (7, 10, 15, 16) (Fig. 1 A.2). The latter step occurs with an unusually high $pK_a > 6$ (17) indicative of the energetic stabilization of the protonated state. Receptor activation thus follows a sequence of thermally activated structural transitions in multiple microdomains which in rhodopsin are spatially and temporally (from ps to ms) separated. The description of the activation process by a hierarchy of structural 'on-off' transitions has originally been based on the spectroscopic identification of inactive rhodopsin states with partial active-like structural features (18) which may cause enhanced thermal receptor activation related to disease (19). Neutralization of the Glu134 side chain has been

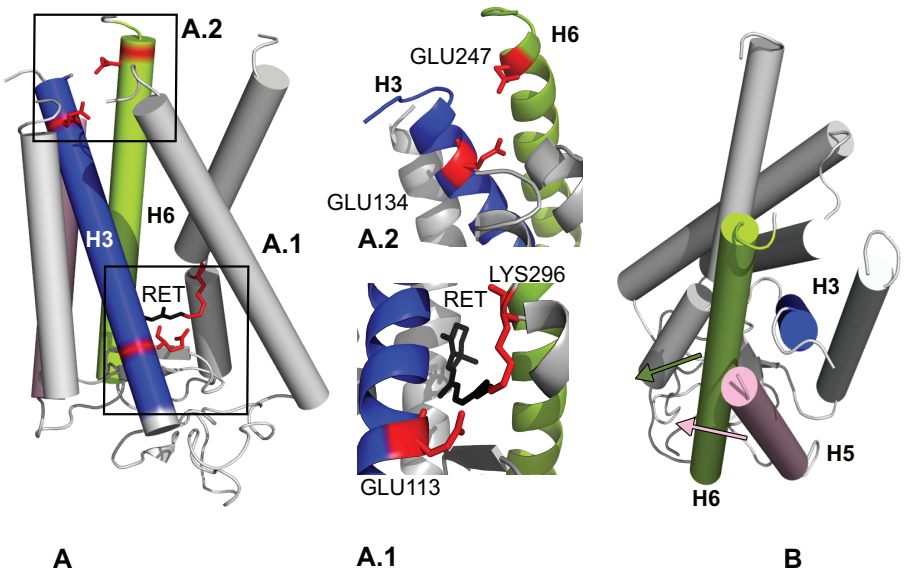

Figure 1: (A) Two proton switches may explain the mechanism of activation of rhodopsin: (A.1) The retinal isomerization produces a transfer of the Schiff base proton to Glu^{113}. (A.2) Glu^{134} positioned in the conserved E(D)RY motif at the C-terminal of TM3 (helix H3) takes up a proton, leading to the $MIIbH^{+}$ intermediate. (B) The hallmark of the transition to active rhodopsin is the movement of helices 6 and 5 (H6, H5) away from H3. See Hofmann *et al.* (2) for details.

identified as one of the crucial activity-promoting factors (20, 21). Although the concept of concerted microdomain switches explains receptor activation (22), the underlying structures are not individually folding units in the strict sense of a protein domain. This raises the question whether short specific sequence motifs of an individually folding TM domain can exhibit local switching processes at all. In the case of the 'proton switch II' at Glu^{134}, it has been argued that the C-terminal end of the isolated TM3 provides an 'autonomous' structural switch that couples protonation to secondary structure formation by side chain partitioning across the lipid water phase boundary (23). Lipid exposure has been suggested to be crucial for this coupling as the protonated side chain would be stabilized by the low dielectric of a bilayer. Whereas the predicted high pK_a of the side chain could be confirmed experimentally, neither the transmembrane topology of the TM3 domain nor the location of secondary structure formation could be determined unequivocally. Furthermore, structural details of the interaction of the Glu^{134} side chain with the sub-headgroup region are not known.

In order to reveal these molecular details, we have performed atomistic molecular dynamics simulations, fluorescence and time-resolved infrared-spectroscopic experiments on lipid-inserted TM3 model peptides. Our data provide a detailed description of proton-induced changes in the secondary structure and topology of TM3. We demonstrate that the pK_a of the Glu^{134} carboxyl is not only tuned by the local dielectric environment at the phase boundary but also by the side chain rotamer state. Finally, the role of the conserved carboxyl group for lipid sub-headgroup

Table 1: **Sequences of TM3 model peptides used in this study.** Bold: position 27 carrying the glutamic acid of the conserved E(D)RY motif of class-A GPCRs. Underlined: additional amino acid replacements which increase helix stability or neutralize the side chain at position 27.

Peptides Names	Sequence
P1	TGCNLEGFFATLGGEIALWSLVVLAI**E**RYVV
P2	TGCNL<u>A</u>GFFATLGG<u>A</u>IALWSLVVLAI**E**RYVV
P3	TGCNL<u>A</u>GFFATLGG<u>A</u>IALWSLVVLAI**Q**RYVV
P4	TGCNL<u>A</u>GFFATLGG<u>A</u>IAL<u>F</u>SLVVLAI**E**RYVW
P5	TGCNL<u>A</u>GFFATLGG<u>A</u>IAL<u>F</u>SLVVLAI**Q**RYVW
P6	TGCNL<u>A</u>GFFATLGG<u>A</u>IAL<u>F</u>SLVV<u>W</u>AI**E**RYVV
P7	TGCNL<u>A</u>GFFATLGG<u>A</u>IAL<u>F</u>SLVV<u>W</u>AI**Q**RYVV
ICL2	AIERYVWVCKPMSNFRFG

hydration is addressed by infrared spectroscopy using both model peptides and Glu^{134}- and Gln^{134}-containing opsin mutants.

Methods

Peptide sequences used in MD calculations. The initial structure of the wild type peptide P1 was derived from the transmembrane helix-3 (TM3) of rhodopsin (pdb entry 1F88, residues 108 – 138) and comprised the amino acids: TGCNLEGFFATLGGEIALWSLVVLAIERYVV. The numbering of all residues is based on the peptide sequence running from T1 to V31. The amino acid Glu^{134} of the native rhodopsin sequence in the conserved E(D)RY motif of class-1 GPCRs corresponds to residue 27 in the peptide models and is designated Glu^{27}. In order to achieve comparability with previous spectroscopic studies, glutamic acids that do not belong to the conserved E(D)RY motif were replaced by alanine in all TM3 peptides investigated here (Table I). In addition to fixing the ionized or protonated state of Glu^{27} in the calculations (systems P1 and P2), peptides with the Glu^{27}Q replacement were studied (system P3). However, spectroscopic studies of these peptides showed that it adopted a mixture of non-helical and helical states which could be avoided by the additional Trp^{19}Phe / Val^{31}Trp double replacement. In order to validate corresponding experimental results, MD simulations were performed for peptides carrying this additional double replacement and a Glu or Gln residue at position 27, respectively (systems P4 and P5). For comparison, MD simulations were also performed with the ICL2 peptide (AIERYVWVCKPMSNFRFG) derived from the second intracellular loop which extends from helix 3. It still carries the conserved E(D)RY motif but lacks the preceding transmembrane segment and was not inserted into a lipidic phase.

Details of MD simulations. Each studied peptide was inserted using the g_membed tool (24) into a system with 128 lipids of 1,2-dioleoyl-sn-glycero-3-phosphocholine (DOPC), and hydrated with 40 water molecules

(TIP3p (25)) per lipid. Peptides with aspartic acid or glutamic acid in the D(E)RY motif, were generated in both protonated and unprotonated states. The Gromacs 4.5.5 package (26) was used and the leap-frog algorithm applied as integrator with a time step of 2 fs. An isothermal-isobaric scheme (NPT) was chosen with the temperature coupled to a heat bath at 303 K, using the Nose-Hoover thermostat with a time coupling constant of 0.5 ps (27, 28). The peptide, the lipid bilayer, and the solvent were coupled separately to the thermostat. The Parrinello-Rahman barostat was used to keep the pressure constant at 1.013 bar, with a time coupling constant of 10.0 ps and an isothermal compressibility of 4×10^5 bar^{-1} (29). The barostat was used with a semi-isotropic scheme, where the pressure in the x-y plane (bilayer plane) and z direction (bilayer normal) were coupled separately. The covalent bonds were constrained with the LINCS (30) and SETTLE (31) algorithms. The long-range electrostatic interactions were treated using the particle mesh Ewald method, with a cut-off in real space of 1.0 nm, and a Fourier spacing of 0.12. The cut-off for van der Waals interactions was chosen to 1.5 nm, using a switch function starting from 1.4 nm. All the systems were simulated using periodic boundary conditions. SLIPIDS (32) and AMBER99 (33) were used as force fields for lipids and peptides, respectively. The systems were minimized using the steepest descent algorithm ($<$ 50,000 steps) and equilibrated for 50 ns with position restraints on the heavy atoms of the peptide. The production simulations were run for 200 ns each.

Infrared spectroscopy of lipid-reconstituted model peptides and opsin mutants. Peptides P6 and P7 were synthesized with C- and N-terminus amidated and acetylated, respectively, HPLC-purified and trifluoroacetate was removed (ThermoFisher, Ulm, Germany). The peptides were reconstituted into vesicles of 1,2-Dioleoyl-sn-Glycero-3-Phosphocholine (DOPC; Avanti Polar Lipids, Inc. Alabaster, USA) by dissolving 10 mg DOPC and 1.5 mg of the peptides in 100-200 μL ethanol followed by solvent evaporation, resolvation in 40 μL ethanol and finally rapid dilution in 1960 μL H_2O (34). Vesicles were formed by at least 10 freeze-thaw cycles of the suspension (35). Rhodopsin mutants carrying the stabilizing Asn^{2}Cys/Asp^{282}Cys amino acid replacements (36) were expressed in HEK-239S cells and detergent-solubilized as described (37), except for using 1% octylglucoside (OG) instead of dodecylmaltoside. These mutants were subsequently purified by using rho-1D4 immunoaffinity chromatography (37). The protein concentration was determined according to Bradford. The solubilized mutant opsins Asn^{2}Cys/Asp^{282}Cys and Asn^{2}Cys/Asp^{282}Cys/Glu^{134}Gln were mixed with DOPC in 1% OG in a 1:100 protein to lipid ratio in a total volume of 200-250 μL. They were simultaneously dialyzed in mini dialysis cups in the identical buffer (1 L of 5 mM phosphate buffer, pH 7.4) with one complete buffer exchange overnight.

The lipid-reconstituted peptide and purified opsin samples were dried on an attenuated total reflectance (ATR) crystal under a gentle stream of nitrogen and hydrated overnight to 85% and 75% relative humidity (r.h.) using a reservoir of a saturated KCl or NaCl solution, respectively (38), separated from the DOPC film by a dialysis membrane and a 1 mm gap of air above the sample. The acquisition of time-resolved Fourier transform infrared

(FTIR) difference spectra induced by hydration has been described in detail (39, 40). Briefly, the r.h. above the sample is increased within 2-4 seconds by a heating current in the salt solution. IR absorption difference spectra are generated from the transmission at defined time intervals after the hydration pulse and the sample transmission at the initial equilibrium hydration. Positive absorption changes are caused by the more hydrated state, negative bands by the initially less hydrated sample. Relaxation of the different samples to the equilibrium hydration took 60 to 180 seconds. An additional waiting time of 5 min was allowed before repeating the experiment in an automated fashion for signal averaging.

Results

Coupling of E^{27} protonation to transmembrane helicity. Previous infrared spectroscopic data on detergent-solubilized TM3 model peptides of bovine rhodopsin supported a protonation-dependent secondary structural transition near the E(D)RY motif in the visual photoreceptor and possibly other GPCRs. However, the extent of helix formation along the sequence and its location relative to the membrane water interface could not be determined. In order to test the proposed pH-regulation of TM3 conformation on a more detailed molecular level, we studied the influence of protonation on the secondary structure of TM3 of rhodopsin using atomistic molecular dynamics (MD) simulations of peptides in a phospholipid bilayer. For comparison with earlier experimental peptide studies using FTIR, CD, and fluorescence spectroscopy (23), a family of related sequences was investigated as well. The peptide P2 (compare Table 1) served as a single transmembrane helical model for the native TM3 sequence and the single carboxyl group in the side chain of E^{27} was chosen to be either protonated or unprotonated in the calculations. Figure 2 A shows the probability for observing the residues of peptide P2 in α-helical conformation. The propensity for α-helix formation was at least 10% higher for the C-terminal end of P2 (residues 20 – 26) in its protonated form as compared to the unprotonated P2 peptide.

For comparison, a simulation was performed for a peptide with the additional $E^{27}Q$ replacement (P3). Such a replacement is generally considered a mimic of the protonated form of a glutamate side chain. However, the helicity in P3 barely exceeded that of P2 in its ionized form. This result suggests that the specific H-bonding properties of a carboxyl group rather than merely its charge state are critically involved in (protonation-dependent) secondary structure formation. The data agree with previous infrared absorption measurements of the protonation-induced C-terminal helix-formation: P2 was incorporated in a detergent micelle, whereas P3 had not been investigated spectrocopically because it formed a large fraction of non-helical structure in detergent. This problem was overcome by the additional $Trp^{126}Phe/Val^{138}Trp$ replacement (residues 24 and 31 in peptides P4, P5) which stabilized the α-helical structure in the experiments (23). Simulations of the corresponding P4 and P5 peptides showed a slightly enhanced α-helical content of the P4 peptide with respect to the wild type sequence (Fig. 2 B). Also for the P4 peptide, a protonation-induced increase of helicity at the C-terminal part was observed. Again, the replacement of

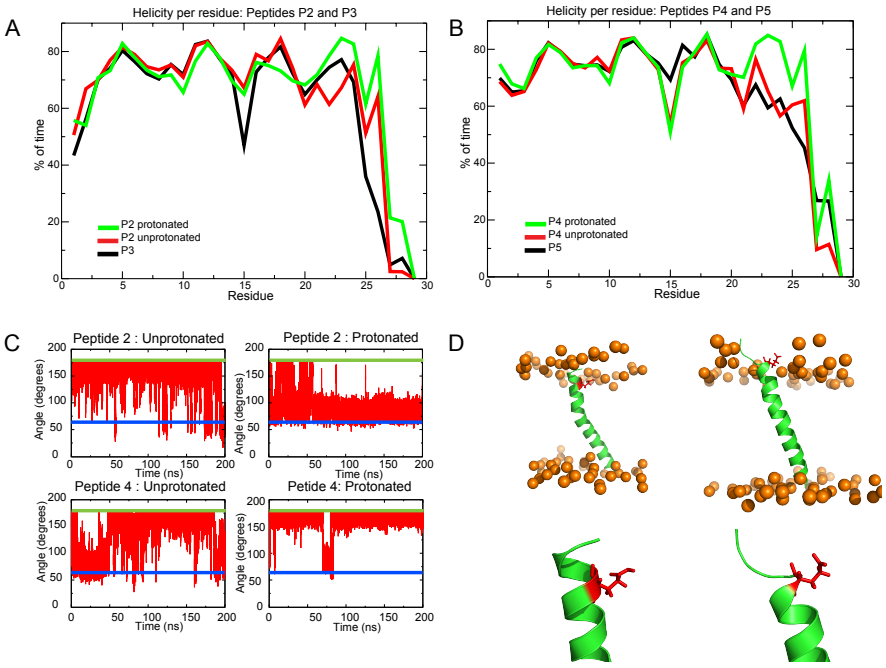

Figure 2: Percentage of helicity per amino acid averaged over 200 ns of simulation. Peptides P2 (A) and P4 (B) were studied in their protonated and unprotonated states and compared with the respective sequences carrying the additional E27Q replacement (P3 and P5, respectively). (C) Dihedral angle $\chi 2$ of glutamic acid as a function of simulation investigated for different peptides. The dihedral angle $\chi 2$ of glutamic acid is represented by red, the blue and green lines mark the cut-off value for gauche and trans conformations, respectively. (D) Upper panel: tansmembrane topology of P4 with E^{27} in the protonated (*left*) and ionized (*right*) state. Lower panel: close up view of the favored protonation-dependent rotamer states of E^{27}.

the titratable amino acid E^{27} by the structurally homologous glutamine residue (P5) did not yield results equivalent to the peptide with protonated E^{27} side chain.

The data agree with the proposed coupling of protonation and conformation at the C-terminus of TM3, but allow to pinpoint the helix stabilization to about five amino acids within the lipidic phase preceding the actual titration site. Furthermore, the data demonstrate that the protonated carboxyl group and the amide group differ significantly in their influence on the peptide structure, despite their common neutral state.

Dynamics of E^{27} side chain conformation. A key assumption of the previously proposed mechanism that couples side chain protonation to conformation is the fluctuation of the Glu^{134} side chain between an 'exposed' and a 'buried' geometry at the membrane interface once the ionic lock is disrupted upon photoactivation of rhodopsin. Therefore, the local peptide structure was further assessed by monitoring fluctuations of the dihedral angle of E^{27} as a function of protonation. Both, the native P2 sequence and the P4 sequence with the C-terminal valine replaced by tryptophan exhibited fluctuations between the gauche and trans conformation of their ionized E^{27} side chain (Fig. 2 C). These fluctuations were strongly reduced upon protonation, leading to the prevalence of the gauche

rotamer for P2, whereas the trans rotamer was stabilized in P4. Thus, although the coupling of protonation to secondary structure formation was identified as a robust feature of the ERY motif (see above), the side chain conformation appears to be further regulated by the sequence context or the peptide insertion depth. Irrespective of this context, however, protonation of both P2 and P4 peptides reduced structural fluctuations. Figure 2 D visualizes the protonation-dependent rotamer preference in the transmembrane topology of P4, showing the position of the gauche rotamer of the ionized carboxyl at the level of the lipid phosphates (*right*), whereas in the protonated state (*left*), the preferred trans isomer locates the carboxyl to the sub-headgroup region.

Protonation-dependent transmembrane positioning of the helical backbone. In addition to helicity and local side chain rotamer preferences, also the insertion depths of the peptides are influenced by the protonation state. The analysis of the membrane insertion depth as a function of sequence position shows that the whole P2 peptide is shifted by ≈ 5 Å towards the N-terminal membrane leaflet upon protonation of Glu^{27} (Fig. 3). For peptide P4 with $Trp^{19}Phe$ and $Val^{31}Trp$ replacements this shift is much less pronounced and only seen for positions close to Glu^{27}. I.e. the interfacial tryptophan-31 firmly anchors the C-terminus of the peptide to the membrane interfacial region. Thus the protonation state of the E(D)RY motif not only controls the local peptide helicity but as well the (local) membrane insertion depth and thus hydrophobicity.

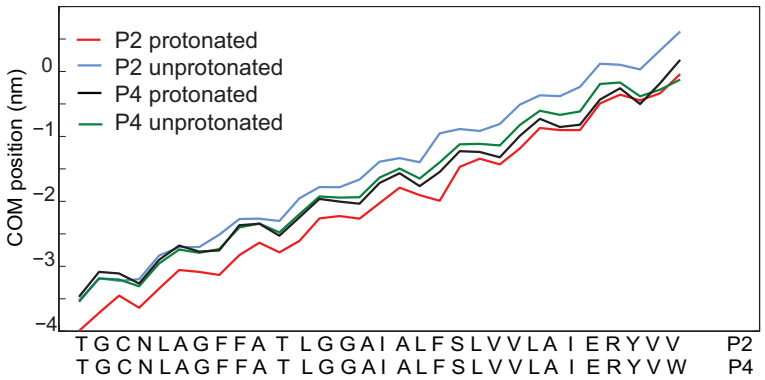

Figure 3: Center of mass (COM) location of amino acids across the lipid bilayer for peptides P2 and P4 for both protonated and unprotonated forms of Glu^{27}. The values were averaged over the final 50 ns of simulation time, the COM of the lipid head groups of the upper monolayer was set to zero.

Coupling of E^{27} side chain pK_a to dielectric environment. The results of a protonation-induced increased membrane insertion depth and increased helicity suggests a dielectric mechanism in the stabilization of the peptide structure and location: The increased hydrophobic immersion of Glu^{134} upon protonation and the coupled lowering of the dielectric constant of its environment may contribute to the high $pK_a > 6$ of Glu^{134} in the proton-dependent equilibrium between MIIa and $MIIbH^+$ states of light-activated rhodopsin (17) and of TM3 model peptides (23).

This hypothesis of an interplay between peptide protonation and localization was addressed by *in silico* analysis of the Glu^{27} pK_a dependency on the dielectric environment.

The pK_a was computed in dependence of two factors: (a) the dielectric constant was varied between 2 and 80, corresponding to the transition between the hydrophobic membrane core and the aqueous phase; (b) the effect of the secondary structure was addressed by computing the pK_a of the Glu^{27} side chain in peptides P2, P4, and for comparison in ICL2. Peptides P2 and P4 have a defined helical structure in a lipid environment. In contrast, the peptide ICL2 is water soluble and corresponds to the N-terminal part of the second intracellular loop of rhodopsin. The pK_a of Glu^{27} in peptides P2 and P4 was observed to strongly depend on both the dielectric environment and the secondary structure: it ranged from 5.2 ($\epsilon = 80$) to more than 10 at $\epsilon < 10$ (Figure 4 A). In contrast, the pK_a of the same side chain in the ICL2 peptide in coiled conformation showed a similar dependency on the dielectric constant, however ranged approximately one unit below the pK_a values of Glu^{27} in P2 and P4.

Thus the increased membrane insertion of the protonated Glu^{27} and the corresponding decrease in dielectric constant can partly explain the elevated pK_a. Additionally, the rotamer states may contribute to pK_a regulation as well: In P2 and P4, the protonated form of Glu^{27} adopts preferentially the gauche and trans rotamer, respectively, and this correlates with an almost constant pK_a difference between the carboxyl in the two peptides over the tested range of dielectric constants. The effect of the rotamer on side chain pK_a is further discussed below.

E^{27} protonation exerts long-range dielectric effects within the bilayer. The MD analysis demonstrated the interdependence of transmembrane topology, local hydrophobicity, side chain protonation and secondary structure. The predicted change in the dielectric environment of the C-terminal end of TM3 as a consequence of protonation-induced repositioning relative to the bilayer was experimentally validated using a peptide with the replacement $Leu^{24}Trp$ (peptide P6). This residue provides a fluorescence monitor by a blue-shift of its emission upon lowering of the local dielectric constant in the majority of proteins (41).

Figure 4 B shows that the tryptophan emission is affected by pH, despite the fact that Trp^{24} is located by a helical turn deeper in the membrane than Glu^{27}. In agreement with the predicted model, the emission of Trp^{24} became blue-shifted upon protonation of Glu^{27}, demonstrating an increased insertion depth into the lipid bilayer. Whereas little pH sensitivity was observed between pH 3 and 6, the blue shift was mainly induced between pH 6 and 7. This confirms the unusually high pK_a of the Glu^{27} side chain carboxyl derived from the theoretical pK_a analysis and also seen for similar TM3 model peptides (23). The pH effect was abolished when Glu^{27} was replaced by Gln (P7 peptide), which further proves the Glu^{27}-mediated molecular mechanism. Emission from Trp^{24} of the P7 peptide was not only pH-insensitive but also observed at shorter wavelength than for P6 (Fig. 4 B, inset). This result indicates a conformational stabilization of the C-terminal part by the neutral Gln side chain as opposed to a side chain that is in equilibrium with an ionized form.

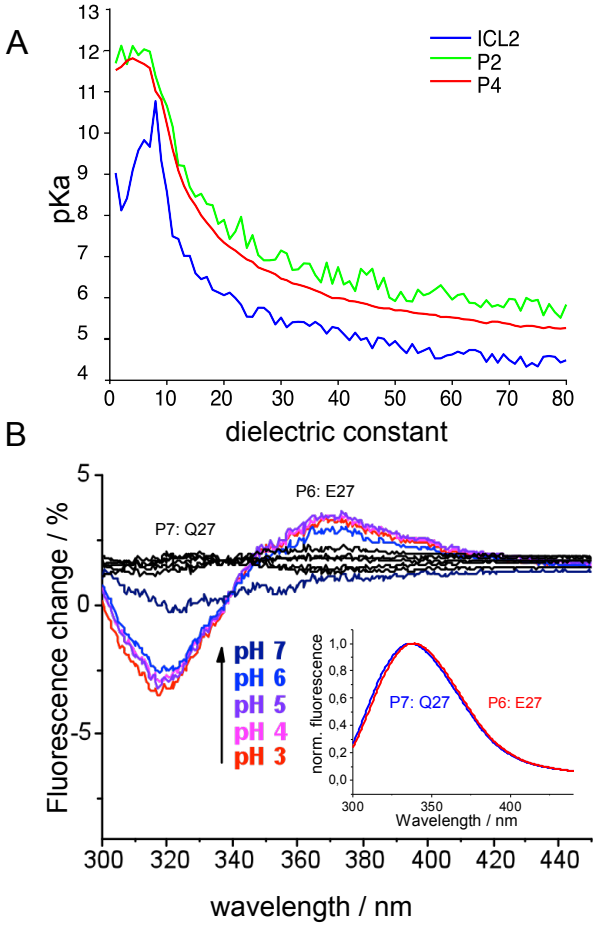

Figure 4: Theoretical and experimental pK_a estimates for Glu^{27}. A) pK_a calculations for Glu^{27} in P2, P4, and ICL2 as a function of the dielectric constant in a homogenous dielectric medium. B) Tryptophan fluorescence of lipid-reconstituted peptides. The displayed pH-dependent spectral shifts were obtained by subtracting the emission spectra taken at the indicated pH values from an emission spectrum recorded at pH 8.8. Thereby, the emission in the ionized state of Glu^{27} in P6 is positive, that of the protonated state is negative (color-coded). The pH sensitivity is abolished in P7 (black). Inset: emission spectra of P6 (red) and P7 (blue) at pH 8.8.

In summary, the MD calculations and tryptophan fluorescence measurements show that the protonation of the Glu^{27} side chain provides a structural switch: The protonation of this site results in a shift of the peptide parallel to the membrane normal that is more pronounced for the non-Trp anchored peptide P2. This protonation-dependent switch observed in the peptide is expected to contribute to the conformation and energetics of the full length receptor. Remarkably, this switch is tailored to the physical constraints of the lipid water phase boundary, such that protonation leads to repositioning of TM3, a reduced flexibility of both the peptide backbone and the side chain of Glu^{27}, and to altered side chain rotamer preferences.

Side chain-dependent dynamics of the sub-headgroup H-bond network. The MD calculations have revealed an unexpected difference between the neutral protonated carboxyl group and the structurally similar amide

group of Gln at position 27 in regulating local secondary structure. Only the protonated carboxyl group stabilized the C-terminal α-helical structure in P2 and P4, whereas Gln^{27} showed this effect in neither peptide. On the other hand, Gln^{27} induced a position shift at Trp^{24}, as did protonation of Glu^{27}.

The only partial mimicking of the protonated state of Glu^{27} by Gln^{27} indicates that in addition to charge, the specific H-bonding geometries of the carboxyl function are required for peptide structure formation. Secondary structure depends on intramolecular backbone H-bonds which compete with intermolecular water H-bonds. Therefore, the interaction of the E(D)RY motif with water in the lipid ester carbonyl region could be crucial for the unique structure induction by a protonated carboxyl rather than an amide. This has motivated us to study the hydration of the DOPC carbonyl region in the presence of P6 and P7.

The infrared absorption of the ester carbonyl stretching mode and the OH-stretching vibration in corresponding lipid films was observed by time-resolved Fourier-transform infrared (FTIR) spectroscopy as a function of hydration. The technique employs a short hydration pulse which increases the relative humidity of air above the lipid film (from 85% RH to 90-95%) within seconds. The experimental setup has been described in detail for the hydration of DNA and lipids (39, 40) and allows to follow the relaxation of the sample to its initial r.h. with seconds time-resolution.

Figure 5 A exemplifies this for a pure DOPC film for which the time-dependent water content was monitored by the absorption change of the OH stretching mode at 3370 cm^{-1}. It is plotted together with the amplitudes of the absorption change of the lipid C=O stretching mode at 1739/1712 cm^{-1}. The curves are averages of 10 such experiments and their perfect superposition demonstrates that the water content and the H-bond strength at the ester carbonyls equilibrated during the entire time-course. This synchronicity was preserved in the presence of P6 (Fig. 5 B), where an additional absorption change at 1663/1650 cm^{-1} revealed changes in peptide bond geometry / H-bonding. Figure 6 A shows the corresponding IR raw data for P7 and compares the C=O hydration response for P6 and P7. Whereas the H-bond-dependent change of the C=O stretching absorption scaled again strictly with hydration for both peptides, the relaxation time for P7 carrying the neutral Gln side chain was faster than for P6. The data show that the presence of the carboxyl function slows down the re-equilibration of lipid-bound water with the gas phase above the lipid film. This supports the critical role of carboxyl-specific H-bonds which need to be broken upon removal of the excess water taken up during transient hydration.

The data raise the question whether the different sub-headgroup hydration properties seen with a carboxyl or amide group at the membrane water interface of DOPC also persist in full length opsins. Opsin mutants carrying the stabilizing $Asn^{2}Cys/Asp^{282}Cys$ double replacement were expressed, reconstituted in DOPC (Methods) and hydrated lipid films adsorbed on an ATR crystal in the same manner used for peptide-containing films. Figure 6 B shows the time-resolved IR raw data for stabilized opsin and a mutant that contains the additional $Glu^{134}Gln$ mutation. Both opsins reproduced the strong synchronicity between water content and ester carbonyl H-bonding, evident from the traces derived from the absorption changes at 3400 cm^{-1} and the 1740/1709 cm^{-1} difference band.

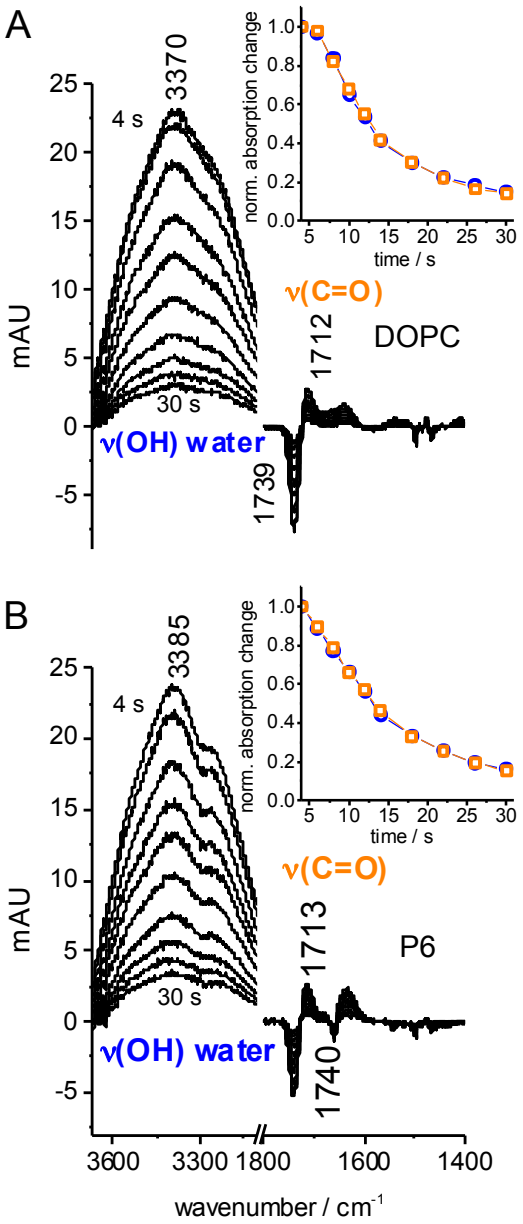

Figure 5: Time-dependent hydration-induced IR absorption changes in DOPC films. A) Decrease of the OH-stretching absorption of water and reduction of the lipid ester C=O stretching absorption difference band over time after the initial absorption changes were induced by a 4 s hydration pulse which increased the r.h. from 75% to 82% in a pure DOPC film. The increased H-bonding to the ester carbonyl led to its frequency downshift which caused the reduction of absorption at 1739 cm^{-1} (disappearance of the less hydrated state) and the increase at 1712 cm^{-1} (appearance of the more hydrated state). With the return to 75% r.h., both the water absorption and the C=O difference band vanish. Inset: reduction of the IR amplitudes at the water OH and lipid ester C=O stretching frequencies over time. B) Equivalent data for a DOPC film containing the peptide P6 (in addition to the absorption changes of water and DOPC, the amide I mode of the peptide also responds to the hydration pulse with a frequency shift in the 1660 to 1640 cm^{-1} range). Color code: ν(C=O): orange, ν(OH) blue.

In contrast to the peptide-containing films, the opsins exhibited a slower re-equilibration of hydration water with the gas phase, reaching the 90% recovery after one minute, rather than 30 s. However, the time courses reveal again

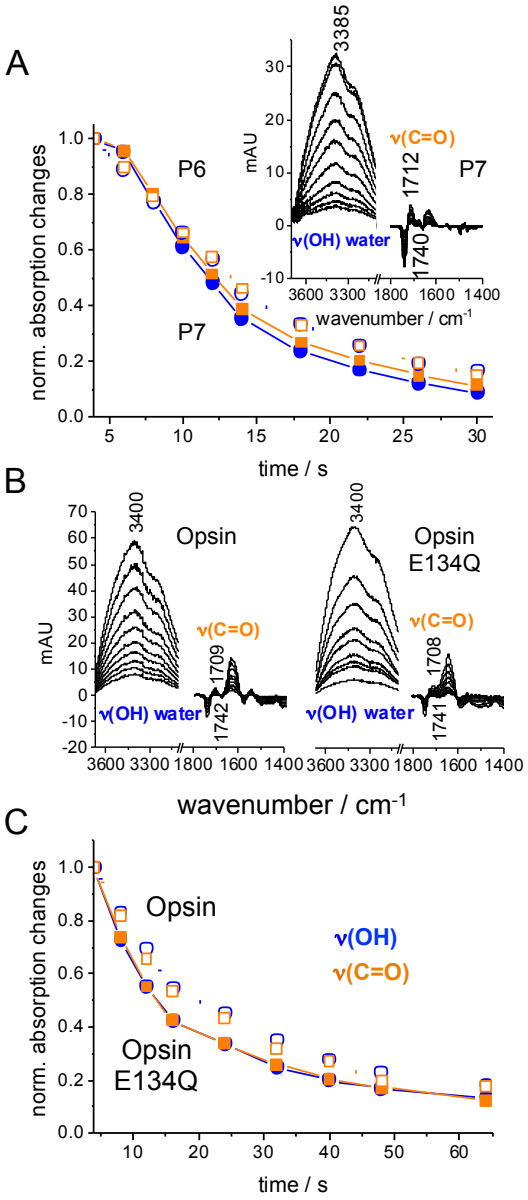

Figure 6: Hydration-induced IR absorption changes in lipid-reconstituted TM3 model peptides and full length opsin mutants. A) Comparison of the relaxation of water OH and lipid ester C=O stretching absorption bands of Glu^{27}- and Gln^{27}-containing peptides P6 and P7, respectively, in DOPC. Inset: the original time-dependent hydration-induced IR difference spectra of P7. B) IR absorption changes induced by hydration of two opsin mutants in DOPC. C) Comparison of the relaxation time course of the water OH (3400 cm^{-1}) and lipid ester C=O stretching absorption changes (around 1741/1709 cm^{-1}) of the opsin mutants reconstituted in DOPC carrying the natural Glu^{134} (opsin) or the Gln^{134} mutation. Color code as in Fig. 5.

a faster water re-equilibration for opsin with the amide-containing side chain at position 134 than with the carboxyl of the native Glu^{134} (Fig. 6 C). The different linkage of membrane hydration to sub-headgroup H-bonding is thus a site-specific feature that prevails in both the full length receptor structure and the TM3 model peptides.

Discussion

Proton-uptake of the conserved E(D)RY motif of the TM3 domain of class A GPCRs is a crucial step in receptor activation. Here, we investigated the influence of protonation on the structure, dynamics, and membrane-insertion of corresponding model peptides in DOPC bilayers using both atomistic molecular dynamics simulations and fluorescence spectroscopy on peptides and full length opsin mutants. A coupling of carboxyl protonation to structural transitions was observed that is suggested to be of functional relevance in the full length receptor.

In active bovine rhodopsin structures (42–44), the side chain of the protonated Glu^{134} in the class-conserved E(D)RY motif does not undergo specific intramolecular interactions. Instead, it resides in a hydrophobic region at the TM3-TM4 interface close to the lipid-facing protein surface. This contrasts the inactive state (45) where its ionized form participates in H-bonding and ionic interactions between Arg^{135} and Glu^{247} on TM6, i.e., the ionic lock that stabilizes the inactive state of the receptor. The MD calculations show that the E(D)RY motif forms a microdomain switch in the true sense: it is part of an independently folding transmembrane domain but adopts protonation-dependent structural sub-states that have counterparts in the crystal structures of inactive and active conformations of rhodopsin. This correspondence concerns in particular the protonation-induced increase in C-terminal helicity, and partially the transition from a *gauche* to a *trans* side chain rotamer for the P4 peptide enforced by the helix anchoring role of Trp^{31}. In agreement with this interpretation, the absence of the Trp^{31} anchor in P2 allows for a more substantial shift of the TM helix toward the C-terminal end when the Glu^{27} side chain becomes ionized.

Membrane anchoring functions have also been described for tyrosines at TM helical ends (46). Remarkably, the potential of the charged side chain of Glu^{27} to promote the TM3 peptide shift is not impeded by the tyrosine of the E(D)RY motif: Tyr^{29} exhibits a three-fold larger displacement in P2 than in the tryptophan-anchored P4 peptide. This agrees with the strong effect of charged residues on TM helical end positioning (47, 48). Nevertheless, for both peptides the ionized state of Glu^{27} favors a shift to the more hydrophilic membrane surface, whereas the protonated glutamic acid is preferentially located in the more hydrophobic sub-headgroup region of the bilayer.

Our data thus show a protonation-dependent partitioning of Glu^{27} in regions of different hydrophobicity. This finding provides a molecular basis for the elevated pK_a of Glu^{134} in the MIIb to $MIIbH^+$ transition of light-activated rhodopsin. The results reveal further mechanistic details that have previously not been considered for the conformational switching process. First, the Glu^{27} pK_a responded differently to the dielectric environment in P2 and P5, revealing a crucial role of the different side chain rotamers for pK_a regulation. Second, a glutamine is generally considered a mimic of a protonated glutamic acid. However, the corresponding replacements made in P3 and P5 did not reproduce the effect of the protonated glutamic acid on stabilizing the C-terminal helical structure. This unexpected result hints at a crucial role of H-bond networks in addition to a side chain positioning within the dielectric gradient at the membrane interface.

Likewise, the rate of sub-headgroup hydration was shown to depend on a single amino acid replacement in the TM3 model peptide. The significant difference in carbonyl dehydration kinetics seen also with the opsin mutants leads us to suggest that the ionized carboxyl is a hydration site at the opsin lipid interface, where proton uptake can lead to more extended remodeling of H-bond networks in the membrane interface. This may explain why in full length rhodopsin in membranes, the Glu^{134}Gln replacement leads to the loss of phosphodiester H-bond interactions normally seen in FTIR difference spectra of the formation of the MII G-protein complex (49). The described importance of the membrane interfacial region in these structural transitions provides a mechanistic rational why Glu^{134} protonation is required for full receptor activation in membranes but not in detergent (50).

In summary, the 'proton switch' mechanism of the E(D)RY motif can be understood on the basis of the dielectric properties of the membrane interface and the membrane-anchoring capability of the sequence context. Correspondingly, the proton-induced structural changes occur in both the isolated microdomain and the full length receptor. In both cases, the side chain carboxyl is additionally connected to the H-bond network in the membrane surface, which is required for secondary structure stabilization.

Author Contributions

RAB and KF designed research, AS performed simulations as well as the simulation analysis, RAB supervised simulation analysis, PR and SM prepared the opsin mutants, SE carried out the spectroscopic measurements, AS, KF, and RAB wrote the manuscript.

Acknowledgement

We would like to thank Kieron South for helping with the expression and purification of the mutant opsins. Angelica Sandoval acknowledges financial support by the Colombian institution Colciencias (scholarship 529/2011). This work was supported by the German Science Foundation (DFG) within the project BO2963/2-1 and the Researchx Training Group 1962 – *Dynamic Interactions at Biological Membranes– From Single Molecules to Tissue* (AS and RAB). Computer time was provided by the Computing Center of the University Erlangen-Nürnberg (RRZE).

References

[1] Lagerstrom, M. C., and H. B. Schioth, 2008. Structural diversity of G protein-coupled receptors and significance for drug discovery. Nat. Rev. Drug Discov. 7:339–357.

[2] Hofmann, K. P., P. Scheerer, P. W. Hildebrand, H. W. Choe, J. H. Park, M. Heck, and O. P. Ernst, 2009. A G protein-coupled receptor at work: the rhodopsin model. TRENDS in Biochem. Sci. 34:540–552.

[3] Palczewski, K., 2006. G Protein-coupled Receptor Rhodopsin. Ann. Rev. Biochem. 75:743.

[4] Ballesteros, J. A., A. D. Jensen, G. Liapakis, S. G. F. Rasmussen, L. Shi, U. Gether, and J. A. Javitch, 2001. Activation of the β_2-Adrenergic Receptor Involves Disruption of an Ionic Lock between the Cytoplasmic Ends of Transmembrane Segments 3 and 6. J. Biomol. Chem. 276:29171–29177.

[5] Shi, L., G. Liapakis, R. Xu, F. Guarnieri, J. A. Ballesteros, and J. A. Javitch, 2002. β2 Adrenergic Receptor Activation Modulation of the Proline Kink in Transmembrane 6 by A Rotamer Toggle Switch. J. Biomol. Chem. 277:40989–40996.

[6] Dror, R. O., D. H. Arlow, D. W. Borhani, M. O. Jensen, S. Piana, and D. E. Shaw, 2009. Identification of two distinct inactive conformations of the β2-adrenergic receptor reconciles structural and biochemical observations. Proc. Natl. Acad. Sci. USA 106:4689–4694.

[7] Sheikh, S. P., T. A. Zvyaga, O. Lichtarge, T. P. Sakmar, and H. R. Bourne, 1996. Rhodopsin activation blocked by metal-ion-binding sites linking transmembrane helices C and F. Nature 383:347–350.

[8] Arnis, S., K. Fahmy, K. P. Hofmann, and T. P. Sakmar, 1994. A Conserved Carboxylic Acid Group Mediates Light-Dependent Proton Uptake and Signaling by Rhodopsin. J. Biomol. Chem. 269:23879–23881.

[9] Mahalingam, M., K. Martínez-Mayorga, M. F. Brown, and R. Vogel, 2008. Two protonation switches control rhodopsin activation in membranes. Proceedings of the National Academy of Sciences 105:17795–17800. http://dx.doi.org/10.1073/pnas.0804541105.

[10] Vogel, R., M. Mahalingam, S. Lüdeke, T. Huber, F. Siebert, and T. P. Sakmar, 2008. Functional Role of the Ïonic Lock¨– An Interhelical Hydrogen-Bond Network in Family A Heptahelical Receptors. J. Molec. Biol. 380:648–655.

[11] Vogel, R., T. P. Sakmar, M. Sheves, and F. Siebert, 2007. Coupling of Protonation Switches During Rhodopsin Activation. Photochem. Photobiol. 83:286–292.

[12] Yan, E. C., M. A. Kazmi, Z. Ganim, J. M. Hou, D. Pan, B. S. Chang, T. P. Sakmar, and R. A. Mathies, 2003. Retinal Counterion Switch in the Photoactivation of the G Protein-Coupled Receptor Rhodopsin. Proc. Natl. Acad. Sci. USA 100:9262–9267.

[13] Jaeger, F., K. Fahmy, T. P. Sakmar, and F. Siebert, 1994. Identification of Glutamic Acid 113 as the Schiff Base Proton Acceptor in the Metarhodopsin II Photointermediate of Rhodopsin. Biochemistry 33:10878–10882.

[14] Standfuss, J., P. C. Edwards, A. D'Antona, M. Fransen, G. Xie, D. D. Oprian, and G. F. Schertler, 2011. The structural basis of agonist-induced activation in constitutively active rhodopsin. Nature 471:656–660.

[15] Farrens, D. L., C. Altenbach, K. Yang, W. L. Hubbell, and H. G. Khorana, 1996. Requirement of rigid-body motion of transmembrane helices for light activation of rhodopsin. Science 274:768–770.

[16] Herrmann, R., M. Heck, P. Henklein, P. Henklein, C. Kleuss, K. P. Hofmann, and O. P. Ernst, 2004. Sequence of Interactions in Receptor-G Protein Coupling. J. Biomol. Chem. 279:24283–24290.

[17] Knierim, B., K. P. Hofmann, O. P. Ernst, and W. L. Hubbell, 2007. Sequence of Late Molecular Events in the Activation of Rhodopsin. Proc. Natl. Acad. Sci. USA 104:20290–20295.

[18] Fahmy, K., F. Siebert, and T. Sakmar, 1995. Photoactivated State of Rhodopsin and How It Can Form. Biophys. Chem. 56:171–181.

[19] Dizhoor, A. M., M. L. Woodruff, E. V. Olshevskaya, M. C. Cilluffo, M. C. Cornwall, P. A. Sieving, and G. L. Fain, 2008. Night Blindness and the Mechanism of Constitutive Signaling of Mutant G90D Rhodopsin. J. Neurosci.. 28:11662–11672.

[20] Cohen, G. B., T. Yang, P. R. Robinson, and D. D. Oprian, 1993. Constitutive Activation of Opsin: Influence of Charge at Position 134 and Size at Position 296. Biochemistry 32:6111–6115.

[21] Kim, J.-M., C. Altenbach, R. L. Thurmond, H. G. Khorana, and W. L. Hubbell, 1997. Structure and Function in Rhodopsin: Rhodopsin Mutants with a Neutral Amino Acid at E134 Have a Partially Activated Conformation in the Dark State. Proc. Natl. Acad. Sci. USA 94:14273–14278.

[22] Nygaard, R., T. M. Frimurer, B. Holst, M. M. Rosenkilde, and T. W. Schwartz, 2009. Ligand Binding and Micro-Switches in 7TM Receptor Structures. TRENDS in Pharm. Sci. 30:249–259.

[23] Madathil, S., and K. Fahmy, 2009. Lipid Protein Interactions Couple Protonation to Conformation in a Conserved Cytosolic Domain of G Protein-coupled Receptors. J. Biomol. Chem. 284:28801–28809. http://dx.doi.org/10.1074/jbc.m109.002030.

[24] Wolf, M. G., M. Hoefling, C. Aponte-Santamaría, H. Grubmüller, and G. Groenhof, 2010. g_membed: Efficient insertion of a membrane protein into an equilibrated lipid bilayer with minimal perturbation. J. Comput. Chem. 31:2169–2174. http://dx.doi.org/10.1002/jcc.21507.

[25] Jorgensen, W. L., J. Chandrasekhar, J. D. Madura, R. W. Impey, and M. L. Klein, 1983. Comparison of simple potential functions for simulating liquid water. J. Chem. Phys. 79:926.

[26] Pronk, S., S. Páll, R. Schulz, P. Larsson, P. Bjelkmar, R. Apostolov, M. R. Shirts, J. C. Smith, P. M. Kasson, and D. van der Spoel, 2013. GROMACS 4.5: a high-throughput and highly parallel open source molecular simulation toolkit. Bioinformatics 29:845–854.

[27] Nosé, S., 1984. A unified formulation of the constant temperature molecular dynamics methods. J. Chem. Phys. 81:511–519.

[28] Hoover, W. G., 1985. Canonical dynamics: equilibrium phase-space distributions. Phys. Rev. A 31:1695–1697.

[29] Parrinello, M., and A. Rahman, 1981. Polymorphic transitions in single crystals: A new molecular dynamics method. J. Appl. Phys. 52:7182–7190.

[30] Hess, B., H. Bekker, H. J. C. Berendsen, and J. G. E. M. Fraaije, 1997. LINCS: A linear constraint solver for molecular simulations. J. Comput. Chem. 18:1463–1472.

[31] Miyamoto, S., and P. A. Kollman, 1992. SETTLE: An analytical version of the SHAKE and RATTLE algorithm for rigid water models. J. Comput. Chem. 13:952–962.

[32] Jämbeck, J. P. M., and A. P. Lyubartsev, 2012. An Extension and Further Validation of an All-Atomistic Force Field for Biological Membranes. J. Chem. Theory Comput. 8:2938–2948.

[33] Hornak, V., R. Abel, A. Okur, B. Strockbine, A. Roitberg, and C. Simmerling, 2006. Comparison of multiple Amber force fields and development of improved protein backbone parameters. PROTEINS: Struc., Func. & Bioinf. 65:712–725.

[34] Krishnakumar, S. S., and E. London, 2007. The Control of Transmembrane Helix Transverse Position in Membranes by Hydrophilic Residues. J. Molec. Biol. 374:1251–1269.

[35] Castile, J. D., and K. M. Taylor, 1999. Factors Affecting the Size Distribution of Liposomes Produced by Freeze-Thaw Extrusion. Int. J. Pharm. 188:87–95.

[36] Standfuss, J., G. Xie, P. C. Edwards, M. Burghammer, D. D. Oprian, and G. F. Schertler, 2007. Crystal Structure of

a Thermally Stable Rhodopsin Mutant. J. Molec. Biol. 372:1179–1188.

[37] Opefi, C. A., K. South, C. A. Reynolds, S. O. Smith, and P. J. Reeves, 2013. Retinitis Pigmentosa Mutants Provide Insight into the Role of the N-terminal Cap in Rhodopsin Folding, Structure, and Function. J. Biomol. Chem. 288:33912–33926.

[38] Rockland, L. B., 1960. Saturated Salt Solutions for Static Control of Relative Humidity Between 5 ° and 40 ° C. Analytical Chemistry 32:1375–1376.

[39] Abusharkh, S. E., C. Erkut, J. Oertel, T. V. Kurzchalia, and K. Fahmy, 2014. The Role of Phospholipid Headgroup Composition and Trehalose in the Desiccation Tolerance of Caenorhabditis Elegans. Langmuir 30:12897–12906.

[40] Khesbak, H., O. Savchuk, S. Tsushima, and K. Fahmy, 2011. The Role of Water H-Bond Imbalances in B-DNA Substate Transitions and Peptide Recognition Revealed by Time-Resolved FTIR Spectroscopy. J. Am. Chem. Soc. 133:5834–5842.

[41] Vivian, J. T., and P. R. Callis, 2001. Mechanisms of Tryptophan Fluorescence Shifts in Proteins. Biophysical Journal 80:2093–2109.

[42] Choe, H., Y. J. Kim, J. H. Park, T. Morizumi, E. F. Pai, N. Krauß, K. P. Hofmann, P. Scheerer, and O. P. Ernst, 2011. Crystal structure of metarhodopsin II. Nature 471:651–655.

[43] Park, J. H., P. Scheerer, K. P. Hofmann, H. W. Choe, and O. P. Ernst, 2008. Crystal structure of the ligand-free G-protein-coupled receptor opsin. Nature 454:183–187.

[44] Scheerer, P., J. H. Park, P. W. Hildebrand, Y. J. Kim, N. Krauß, H. W. Choe, K. P. Hofmann, and O. P. Ernst, 2008. Crystal structure of opsin in its G-protein-interacting conformation. Nature 455:497–502.

[45] Palczewski, K., T. Kumasaka, T. Hori, C. A. Behnke, H. Motoshima, B. A. Fox, I. Le Trong, D. C. Teller, T. Okada, R. E. Stenkamp, M. Yamamoto, and M. Miyano, 2000. Crystal Structure of Rhodopsin: A G Protein-coupled receptor. Science 289:739–745. http://dx.doi.org/10.1126/science.289.5480.739.

[46] Gleason, N. J., V. V. Vostrikov, D. V. Greathouse, C. V. Grant, S. J. Opella, and R. E. Koeppe, 2012. Tyrosine Replacing Tryptophan as an Anchor in GWALP Peptides. Biochemistry 51:2044–2053.

[47] Shahidullah, K., S. S. Krishnakumar, and E. London, 2010. The Effect of Hydrophilic Substitutions and Anionic Lipids Upon the Transverse Positioning of the Transmembrane Helix of the Erbb2 (Neu) Protein Incorporated into Model Membrane Vesicles. Journal of Molecular Biology 396:209–220.

[48] Lew, S., J. Ren, and E. London, 2000. The Effects of Polar and/or Ionizable Residues in the Core and Flanking Regions of Hydrophobic Helices on Transmembrane Conformation and Oligomerization. Biochemistry 39:9632–9640.

[49] Fahmy, K., T. P. Sakmar, and F. Siebert, 2000. Transducin-dependent protonation of glutamic acid 134 in rhodopsin. Biochemistry 39:10607–10612.

[50] Lüdeke, S., M. Mahalingam, and R. Vogel, 2009. Rhodopsin activation switches in a native membrane environment. Photochem. and Photobiol. 85:437–441.